Published in final edited form as:
Bioorg Med Chem. 2011 June 1; 19(11): 3425–3433. doi:10.1016/j.bmc.2011.04.029.

Synthesis and preliminary evaluation of radiolabeled bis(zinc(II)-dipicolylamine) coordination complexes as cell death imaging agents

Leonie wyffels[a,d], **Brian D. Gray**[b], **Christy Barber**[a], **James M. Woolfenden**[a], **Koon Y. Pak**[b], and **Zhonglin Liu**[a,*]

[a] Department of Radiology, University of Arizona, Tucson, AZ, USA

[b] Molecular Targeting Technologies, Inc. West Chester, PA, USA

[c] Department of Chemistry and Biochemistry, University of Notre Dame, Notre Dame, IN, USA

Abstract

The aim of this study was the development of ^{99m}Tc labeled bis(zinc(II)-dipicolylamine) (Zn^{2+}-DPA) coordination complexes, and the in vivo evaluation of their usefulness as radiotracers for the detection of cell death. DPA ligand **1** was labeled with ^{99m}Tc via the ^{99m}Tc-tricarbonyl core ([^{99m}Tc(CO)$_3$-**1**]$^{3+}$) or via HYNIC (^{99m}Tc-HYNIC-**1)** in good radiochemical yields. Highest in vitro stabilities were demonstrated for [^{99m}Tc(CO)$_3$-**1**]$^{3+}$. A mouse model of hepatic apoptosis (anti-Fas mAb) was used to demonstrate binding to apoptotic cells. ^{99m}Tc-HYNIC-**1** showed the best targeting of apoptotic hepatic tissue with a 2.2 times higher liver uptake in anti-Fas treated mice as compared to healthy animals. A rat model of ischemia-reperfusion injury was used to further explore the ability of the ^{99m}Tc-labeled Zn^{2+}-DPA coordination complexes to target cell death. Selective accumulation could be detected for both tracers in the area at risk, correlating with histological proof of cell death. Area at risk to normal tissue uptake ratios were 3.82 for [^{99m}Tc(CO)$_3$-**1**]$^{3+}$ and 5.45 for ^{99m}Tc-HYNIC-**1**.

1. Introduction

Cell death can result from two different but closely related processes, apoptosis and necrosis. Apoptosis or programmed cell death plays a key role not only in normal tissue homeostasis but also in the etiology and pathology of a plethora of diseases. Pathologies associated with too much apoptosis include AIDS,[1] organ transplant rejection,[2] neurodegenerative disorders such as Alzheimer's disease,[3] and cardiovascular diseases such as ischemia-reperfusion injury.[4] Too little apoptosis, on the other hand, can lead to the development of cancer.[5] Besides its participation in disease, apoptosis may also play an important role in disease treatment. Anti-cancer therapies including chemotherapy and radiation therapy function by promoting apoptosis in the target cells.[6] Necrosis, on the other hand, results from physiological damage and sudden metabolic failure.[7] It is a disorganized,

*Corresponding author: Tel: +1 (520) 626-4248; Fax: +1 (520) 626-2892, zliu@radiology.arizona.edu.
[d]Permanent address: University Hospital Antwerp, Wilrijkstraat 10, B-2650 Oedeem (Antwerp), Belgium

passive form of cell death, characterized by swelling and rupture of the cell membrane, resulting in activation of an inflammatory response.

Molecular imaging of cell death processes can be a very useful tool to assist in diagnosis of disease, monitoring of disease course and treatment evaluation, as well as in development and evaluation of new drugs. Currently, most apoptotic cell death imaging approaches are based on targeting phosphatidylserine (PS). In most cells, PS is maintained almost exclusively in the inner monolayer of the cell membrane. A hallmark of apoptosis is the externalization of phosphatidylserine (PS) to the outer side of the plasma membrane.[8] When cells become apoptotic, translocase and floppase that normally keep PS inwards become deactivated while a third enzyme called scramblase is activated.[9] This results in a redistribution of phospholipids across the bilayer and consequent externalization of PS to the outer leaflet of the cell membrane. The appearance of PS on the cell membrane surface is an early sign that the cell death program has been activated,[10] and serves as a signal for phagocytosis and removal.[11] Since PS is an anionic phospholipid, the externalization alters the cell surface charge to negative.[11,12] In necrotic cells, PS becomes accessible due to passive rupture of the cell membrane. The presence of PS on the cell surface provides an abundant molecular marker for detection of apoptotic and necrotic cells.

The most well known tracers for the detection of apoptosis based on targeting of externalized PS are based on annexin V. Annexin V is a member of the annexin protein family and is known to bind with high affinity to PS in a Ca^{2+} dependent manner.[13,14] Consequently, annexin V conjugates have been developed for in vitro and in vivo detection of apoptosis and necrosis.[7] Several radiolabeled derivatives of annexin V have been developed for PET (^{18}F, ^{68}Ga, ^{124}I),[15–17] and SPECT (^{99m}Tc, ^{123}I)[18,19] imaging of cell death. Although radiolabeled annexin V derivatives remain under extensive investigation, their current in vivo usefulness is found to be limited. Low target-to-background ratios, and long biological half-life with high uptake in liver and kidney initiated the development of conjugates with better biodistribution profiles.[7] Although derivatives of annexin V continue to evolve, the so-called second generation design is limited for protein-based probes like annexin V.

Low-molecular weight probes are more amenable to structural optimization and display more favorable pharmacokinetic properties compared to protein-based probes like annexin V. Recently, Smith et al. discovered that rationally designed bis(zinc(II)-dipicolylamine) (Zn^{2+}-DPA) coordination complexes can mimic the apoptosis sensing function of annexin V.[20] Two meta-oriented Zn^{2+}-DPA units are responsible for PS recognition and binding.[21] Commercially available PSVue®794, with a Zn^{2+}-DPA affinity group conjugated to a near-infrared carbocyanine fluorophore (ex. 794 nm, ex. 810nm), was shown to selectively stain the same cells as fluorescently labeled annexin V in cell culture.[22] It was also demonstrated that the probe selectively binds to anionic surfaces of bacteria and can be used for in vivo imaging of bacterial infection in mice.[23,24] Furthermore, PSVue®794 can be used for in vivo imaging of necrotic regions in prostate and mammary tumor xenografts.[22] Although NIR fluorophores are very useful for a wide array of preclinical small animal imaging studies, clinical translation remains at a proof-of-principle stage.[25] The use of radioisotopes and positron emission tomography (PET) and single photon emission computed tomography (SPECT) imaging are more suited for deep tissue imaging and clinical application. Since no radiolabeled Zn^{2+}-DPA coordination complex tracers have been described so far, the aim of this study was radiolabeling of a Zn^{2+}-DPA coordination complex (**1**) with SPECT isotope ^{99m}Tc and preliminary in vivo and ex vivo evaluation of the usefulness of the new radiotracers for detection of apoptosis and necrosis.

2. Results and discussion

2.1. Radiolabeling

Two radiolabeled compounds were prepared, $[^{99m}Tc(CO)_3$-**1**$]^{3+}$ and ^{99m}Tc-HYNIC-**1** (Fig. 1). The $[^{99m}Tc(CO)_3]^+$ core was chosen for labeling because of its simple aqueous chemistry. Tridentate chelates like the dipicolylamine chelate moiety have been shown to readily react with the $[^{99m}Tc(CO)_3]^+$ core to result in chemically robust complexes.[26] The thermodynamic stability of the complexes limits the presence of radiolabeled metabolites that may seriously hamper in vivo imaging and quantification of the original tracer.[27] HYNIC (2-hydrazinonicotinic acid), on the other hand, is one of the most popular and efficient bifunctional chelators for ^{99m}Tc-labeling of different groups of molecules.[28] Therefore the HYNIC methodology was chosen as an alternative strategy for ^{99m}Tc-labeling of compound **1**.

In order to label the dipicolylamine subunits in compound **1** with ^{99m}Tc, the $[^{99m}Tc(H_2O)_3(CO)_3]^+$ precursor was first prepared by addition of $^{99m}TcO_4^-$ to an Isolink kit. Incubation of compound **1** (Fig. 1) with $[^{99m}Tc(H_2O)_3(CO)_3]^+$ at 100 °C for 20 min resulted in $[^{99m}Tc(CO)_3$-**1**$]^{3+}$ in ≥ 95 % radiochemical yields. The concentration of compound **1** needed to be 1 mM to achieve these high yields. Reverse phase HPLC (RP-HPLC) analysis of the reaction mixture is presented in Fig. 2. $[^{99m}Tc(CO)_3$-**1**$]^{3+}$ elutes from the column with a retention time (t_R) of 12.9 min. Following Sep-Pak purification, radiochemical purities were consistently ≥ 98 % by RP-HPLC analysis.

HYNIC-**1** was prepared by reacting compound **1** with the N-hydroxysuccinimide (NHS) active ester of HYNIC in a 1:1 molar ratio for 90 min at room temperature. Longer reaction times (overnight) or higher concentrations of NHS-HYNIC did not significantly increase the yield. Following purification, the identity of HYNIC-**1** was confirmed by mass spectrometry (MS) analysis. ^{99m}Tc-HYNIC-**1** was prepared using conditions similar to those previously described.[29] HYNIC-**1** was reacted with $^{99m}TcO_4^-$ in the presence of stannous chloride and nicotinic acid/tricine as coligand system at 90 °C for 20 min. HPLC analysis of the reaction mixture revealed a high labeling efficiency with < 2 % of $[^{99m}$Tc]-pertechnetate (t_R = 4.8 min) present (Fig. 2). However, besides the main peak with a t_R of 15.3 min (approx. 80 %), some additional later-eluting peaks (18.0 and 21.6 min, approx. 20 % total) were observed that may be related to isomerism or various numbers of coligands. The presence of acetonitrile (MeCN) in the mobile phase used for HPLC analysis can also result in mixed tricine/MeCN coligand complexes on the column that are not present in the sample under analysis.[30] HPLC purification of ^{99m}Tc-HYNIC-**1** (isolation of the main peak at t_R of 14.9 min) did not significantly change in vivo behavior (data not presented). Therefore, no attempts were yet made to optimize the radiolabeling procedure. The radiolabeling yield varied between 60 and 79 %.

2.2. In vitro stability and distribution coefficient

$[^{99m}Tc(CO)_3$-**1**$]^{3+}$ and ^{99m}Tc-HYNIC-**1** were analyzed by RP-HPLC for stability after incubation in saline at room temperature and serum at 37 °C for 20 h. The results are summarized in Table 1. The tracers were analyzed for stability after addition of $Zn(NO_3)_2$. The added Zn^{2+} did not seem to compete with the radioisotopes for complexation. $[^{99m}Tc(CO)_3$-**1**$]^{3+}$ showed a high stability towards incubation in saline and serum with ≥ 98 % intact $[^{99m}Tc(CO)_3$-**1**$]^{3+}$ after 20 h of incubation. ^{99m}Tc-HYNIC-**1** (main peak approx. 80 % at 0 h) was found to be less stable in saline and serum (72 % and 67 %, respectively at 20 h). The main impurity that could be detected was free ^{99m}Tc in the form of pertechnetate eluting at a t_R of 4.8 min. A challenge experiment with cysteine was also done. The radiochemical purity of $[^{99m}Tc(CO)_3$-**1**$]^{3+}$ remained unchanged when incubated in 100 mM

cysteine solution for 20 h. The stability of ^{99m}Tc-HYNIC-**1** towards cysteine challenge was lower. The area under the main peak diminished (56 % at 20 h) while a peak at t_R 4.8 min (6% at 20 h) and a peak at t_R 8.4 min (17% at 20 h) increased. The decrease in radiochemical purity can probably be related to transchelation to cysteine.

The distribution coefficient of the tracers was determined in a mixture of *n*-octanol and phosphate buffered saline (PBS, pH 7.4). LogD values of −0.22 ± 0.01 and −2.30 ± 0.01 were measured for $[^{99m}Tc(CO)_3$-**1**$]^{3+}$ and ^{99m}Tc-HYNIC-**1**, respectively. The lower hydrophilicity of $[^{99m}Tc(CO)_3$-**1**$]^{3+}$ can be assigned to the $^{99m}Tc(CO)_3$-core which is known to increase the hydrophobicity of complexes.[31,32]

2.3. Biodistribution study in normal mice

A biodistribution study in normal BALB-c mice was done to determine the influence of the ^{99m}Tc labeling strategy on tracer tissue distribution. The distribution of radioactivity in various tissues as a function of time following intravenous (iv) administration of $[^{99m}Tc(CO)_3$-**1**$]^{3+}$and ^{99m}Tc-HYNIC-**1** is represented in Fig. 3. Both tracers showed rapid blood clearance with $[^{99m}Tc(CO)_3$-**1**$]^{3+}$ demonstrating the fastest clearance (0.3 ± 0.1 % injected dose (ID)/g versus 3.6 ± 0.3 %ID/g in blood at 1 h post injection (pi) for $[^{99m}Tc(CO)_3$-**1**$]^{3+}$and ^{99m}Tc-HYNIC-**1**, respectively). This rapid blood clearance may substantially reduce background activity in imaging studies, but might interfere with localization of the tracer at the target site. For both tracers, the highest uptake was in liver and intestines. Liver uptake remained high throughout the study for $[^{99m}Tc(CO)_3$-**1**$]^{3+}$ (31.5 ± 2.8 %ID/g at 15 min and 19.3 ± 1.8 %ID/g at 24h pi). ^{99m}Tc-HYNIC-**1** showed an initial high liver uptake (22.0 ± 2.8 %ID/g at 15 min pi), followed by a continuous decrease until the end of the study (4.5 ± 0.8 %ID/g at 24 h pi). The higher liver retention of $[^{99m}Tc(CO)_3$-**1**$]^{3+}$ might be associated with the somewhat higher lipophilicity of the compound compared to ^{99m}Tc-HYNIC-**1**. High liver uptake associated with the $^{99m}Tc(CO)_3$-core has been previously described by others.[26, 27, 32] However, since the logP value of $[^{99m}Tc(CO)_3$-**1**$]^{3+}$ indicates only low lipophilicity, logP value is most likely only one of the determining factors in the liver retention of $[^{99m}Tc(CO)_3$-**1**$]^{3+}$. Other factors like binding to plasma proteins, overall charge and complex stericity may govern the non-specific liver retention.

Only minor uptake could be detected for both tracers in kidneys (3.6 ± 0.4 %ID/g at 1 h pi and 2.1 ± 0.1 %ID/g at 4 h pi for $[^{99m}Tc(CO)_3$-**1**$]^{3+}$ and 2.3 ± 0.8 %ID/g at 1 h pi and 1.2 ± 0.2 %ID/g at 4 h pi for ^{99m}Tc-HYNIC-**1**) and in urine (2.1 ± 1.7 %ID at 1 h pi and 0.03 ± 0.03 %ID at 4 h pi for $[^{99m}Tc(CO)_3$-**1**$]^{3+}$ and 2.4 ± 3.3 %ID at 1 h pi and 0.2 ± 0.2 %ID at 4 h pi for ^{99m}Tc-HYNIC-**1)** indicating clearance of both tracers mainly through the hepatobilary system. A higher uptake in lungs could be detected for ^{99m}Tc-HYNIC-**1** compared to $[^{99m}Tc(CO)_3$-**1**$]^{3+}$ (2.3 ± 0.6 %D/g and 1.0 ± 0.3 %ID/g at 1 h pi for ^{99m}Tc-HYNIC-**1** and $[^{99m}Tc(CO)_3$-**1**$]^{3+}$, respectively). Low and comparable uptake could be detected in stomach and muscle for both tracers. Compared to ^{99m}Tc-labeled forms of annexin V, both tracers showed lower kidney uptake and faster blood clearance.[19] This faster blood clearance was to be expected considering the lower molecular weight of our tracers compared to annexin V tracers. Liver uptake, on the other hand, was higher for both DPA compounds compared to ^{99m}Tc-labeled annexin V. Low-molecular weight probes like the Zn^{2+}-DPA coordination complexes however, in contrast to large protein ligands like annexin V, are more amenable to second generation design to lower the unfavorable liver uptake and improve the imaging characteristics.[33]

2.4. Tracer uptake in mice with Fas-mediated hepatic apoptosis

A well-described in vivo model of programmed cell death[19,34,35] was used to determine the targeting properties of [^{99m}Tc(CO)$_3$-**1**]$^{3+}$ and ^{99m}Tc-HYNIC-**1** for in vivo apoptotic cells. Fas is a cell-surface receptor belonging to the death-receptor family.[36] Intravenous administration of an agonistic anti-Fas mAb will induce rapid and massive hepatic apoptosis.[34] To demonstrate presence of apoptosis, routine H&E staining and immunohistological analysis using a rabbit anti-cleaved caspase-3 was performed on 3 μm slices of control and anti-Fas treated livers. Livers of control mice did not show any staining of cleaved caspase-3, a biological indicator of early apoptosis (Fig. 4). On the other hand, high levels of stained cleaved caspase-3 were detected in the livers of mice treated with anti-Fas mAb, indicating the presence of massive hepatic apoptosis. Tracer uptake in livers of control mice and anti-Fas treated mice was analyzed by planar scintigraphy, γ-counting and by autoradiography. Consistent with the results obtained in the biodistribution study in healthy mice, the highest uptake was detected in livers of mice injected iv with [^{99m}Tc(CO)$_3$-**1**]$^{3+}$ (Fig. 5). Uptake of [^{99m}Tc(CO)$_3$-**1**]$^{3+}$ was significantly ($p < 0.05$) higher (1.73 times) in livers of mice treated with anti-Fas mAb (43.23 ± 9.43 %ID/g) compared to controls (26.85 ± 3.88 %ID/g). A 2.2 times higher uptake was detected in livers of anti-Fas mAb treated mice (19.60 ± 1.72 %ID/g) injected with ^{99m}Tc-HYNIC-**1** as opposed to livers of control mice (8.97 ± 2.80 %ID/g) (Fig. 4 and Fig. 5). The results are comparable to the increase in liver uptake described for ^{99m}Tc-labeled annexin V derivatives[19,37] and indicate in vivo affinity of [^{99m}Tc(CO)$_3$-**1**]$^{3+}$ and ^{99m}Tc-HYNIC-**1** for hepatic apoptosis. The best results are obtained for ^{99m}Tc-HYNIC-**1** and can be explained by a difference in binding strength. Like fluorescent Zn^{2+}-DPA coordination complexes,[20, 38] ^{99m}Tc-HYNIC-**1** presumably binds to PS on the surface of apoptotic cells through coordination interactions between the two zinc ions and the carboxylate and the phosphate anions of the PS headgroup. In [^{99m}Tc(CO)$_3$-**1**]$^{3+}$, on the other hand, one of the zinc ions is replaced by a ^{99m}Tc-tricarbonyl core. This saturated coordination complex can only interact with the PS headgroups through weaker electrostatic interactions, resulting in a lower affinity. Although reasonably selective binding of anionic membranes has been reported for compounds containing just a single Zn^{2+}-DPA unit,[38] the affinity would still be lower compared to ^{99m}Tc-HYNIC-**1** containing two Zn^{2+}-DPA binding units.

The increase in liver uptake in anti-Fas treated mice might be related to tissue damage caused by the anti-Fas mAb. Therefore, inactivated control compounds with a minimally altered structure and the molecular weight of [^{99m}Tc(CO)$_3$-**1**]$^{3+}$ and ^{99m}Tc-HYNIC-**1** are desirable to further investigate non-specific uptake.

2.5. Ex-vivo specificity for myocardial ischemia-reperfusion injury

A rat model of myocardial ischemia-reperfusion injury was used as a second animal model to demonstrate sensitivity of the ^{99m}Tc-labeled tracers for apoptotic and necrotic tissue. Cell death in this clinical situation occurs both in the ischemia as well as the reperfusion phase. H&E staining of the heart slices demonstrated cell damage in the area at risk, characterized by contraction bands, wavy fibers, congestion of red blood cells and in some areas polymorphonuclear cell infiltration, indicating early inflammation. Only few apoptotic cells could be demonstrated by cleaved caspase-3 staining. This is in contrast to previously reported studies that could demonstrate the presence of apoptotic cells in prolonged ischemia-reperfusion injury, using different detection methods.[39–41] Selective accumulation of radioactivity in the area at risk undergoing cell death could be observed for both tracers on autoradiograms of myocardial sections (Fig. 6). Area at risk to normal tissue uptake ratios were 3.82 for [^{99m}Tc(CO)$_3$-**1**]$^{3+}$ and 5.45 for ^{99m}Tc-HYNIC-**1**. These values are comparable to those described for ^{99m}Tc-labeled annexin V derivatives using similar rat models of myocardial ischemia-reperfusion injury.[40, 42] Although the uptake in the area at

risk was significantly higher ($p < 0.05$) than in normal myocardium for both tracers, values are too low (0.15 ± 0.07 %ID/g in area at risk and 0.04 ± 0.02 %ID/g in normal myocardium for $[^{99m}Tc(CO)_3$-**1**$]^{3+}$, 0.12 ± 0.03 %ID/g in area at risk and 0.02 ± 0.00 %ID/g in normal myocardium for ^{99m}Tc-HYNIC-**1**) for in vivo SPECT imaging. Also, compared to the total myocardial uptake (0.10 ± 0.03 %ID/g and 0.06 ± 0.01 %ID/g for $[^{99m}Tc(CO)_3$-**1**$]^{3+}$ and ^{99m}Tc-HYNIC-**1**, respectively), high liver uptake was present (2.58 ± 0.34 %ID/g and 0.76 ± 0.10 %ID/g for $[^{99m}Tc(CO)_3$-**1**$]^{3+}$ and ^{99m}Tc-HYNIC-**1**, respectively). This liver uptake could seriously hamper in vivo imaging due to a high background signal, limiting the usefulness of the tracers for in vivo imaging of myocardial ischemia-reperfusion injury. It must be noted that even though both tracers show selective accumulation in the area at risk, this does not necessarily warrant interaction with apoptotic or necrotic cells. Myocardial injury is known to be associated with vascular hyperpermeability and increased interstitional space.[43,44] Therefore uptake in the area at risk might also be associated with passive diffusion of the tracer in parallel with specific uptake. Further research using a non-selective inactivated probe will be needed to characterize this non specific uptake.

3. Conclusion

The aim of this study was to synthesize radiolabeled Zn^{2+}-DPA coordination complexes and characterize their potential as tracers for in vivo detection of cell death. Zn^{2+}-DPA coordination complex **1** was successfully radiolabeled with ^{99m}Tc via $^{99m}Tc(CO)^{3+}$ or via HYNIC to form $[^{99m}Tc(CO)_3$-**1**$]^{3+}$ and ^{99m}Tc-HYNIC-**1**, respectively. The hepatic apoptosis model suggests that both $[^{99m}Tc(CO)_3$-**1**$]^{3+}$ and ^{99m}Tc-HYNIC-**1** target cells undergoing cell death. Selective accumulation of $[^{99m}Tc(CO)_3$-**1**$]^{3+}$ and ^{99m}Tc-HYNIC-**1** was observed in myocardial ischemia-reperfusion injury. However, the absolute tracer uptake in the myocardium with ischemia-reperfusion injury remained low and might be less detectable by in vivo cardiac imaging. Further research is needed to enhance the tracer uptake in the apoptotic/necrotic tissue and to reduce the liver accumulation. In addition, further studies using other in vitro and in vivo models of cell death are necessary to determine the binding affinity and exact binding mechanism to apoptotic and necrotic cells. Labeling with other radioisotopes such as ^{111}In for SPECT imaging, and ^{68}Ga, ^{18}F and ^{11}C for PET imaging should be investigated to further explore the potential of radiolabeled Zn^{2+}-DPA coordination complexes for in vivo detection of cell death.

4. Experimental

4.1. General procedures and materials

Chemicals were purchased from Sigma-Aldrich Chemical Company unless otherwise stated and used as they were received. Pertechnetate ($^{99m}TcO_4^-$) eluted from a ^{99}Mo-^{99m}Tc generator, was purchased from GE Healthcare (Phoenix, AZ). IsoLink kits for the preparation of $[^{99m}Tc(H_2O)_3(CO)_3]^+$ were kindly provided by Covidien (St Louis, MO). Mass spectrometry was performed on a Thermo-Finnigan (San Jose, CA) LCQ mass-spectrometer with electrospray-ionization probe. ^{1}H nuclear magnetic resonance (NMR) spectrometry was performed on a Bruker DRX-600 spectrometer (Department of Chemistry, University of Arizona). Chemical shifts were recorded in ppm (δ) from an internal tetramethylsilane standard in chloroform-d_3. High performance liquid chromatography (HPLC) purification and analyses of the compounds were performed using a Waters Breeze system (Waters Corp., Milford, MA) equipped with a Waters 1525 binary pump, Waters 2489 UV/VIS detector (λ = 254 nm and 260 nm) in series with a Bioscan B-FC-1000 radiodetector (Bioscan Inc., Washington, DC). Radioactivity of samples was measured in a well counter. High-activity samples were measured in an ionization chamber dose calibrator (Capintec CRC, Ramsey, NJ). Autoradiograms were obtained using a FujiFilm BAS5000 Bio-Imaging Analysis System (Fujifilm Medical Systems U.S.A., Inc., Stamford, CT) and

were analyzed using Multi-Gauge 3.0 software. The animal experiments were performed in accordance with the Principles of Laboratory Animal Care from the National Institutes of Health (NIH Publication 85–23, revised 1985) and were approved by the Institutional Animal Care and Use Committee (IACUC) at the University of Arizona.

4.2. Synthesis

4.2.1. N,N′-(5-(4-aminobutoxy)-1,3-phenylene)bis(methylene)bis(1-(pyridine-2-yl)-N-(pyridine-2-ylmethyl)methanamine) (1)—Compound **1** was synthesized as previously described.[45]

4.2.2. Hydrazinonicotinamido-1 (HYNIC-1)—HYNIC conjugated **1** was synthesized by reacting succinimidyl 6-hydraziniumnicotinate hydrochloride (NHS-HYNIC) (Solulink, Inc. San Diego, Ca) with **1** in a 1:1 ratio. **1** (2 mg, 3.4 μmol) was dissolved in a mixture of MeCN (50 μL), DMF (50 μL) and 0.1M HEPES (400 μL). To this solution NHS-HYNIC (3.4 μmol, 0.975 mg dissolved in 100 μL anhydrous DMF) was added dropwise. The reaction was stirred for 90 min at room temperature, protected from light. The reaction was stopped by addition of 1 mL H_2O and the reaction mixture was sent over a C18 Sep-Pak cartridge (Waters Corp., Milford, MA) washed with 5 mL of H_2O, and eluted with 1 mL of ethanol. The solution was evaporated to dryness and the residue dissolved in 100 μL MeCN and purified by RP-HPLC (BioAdvantage Pro300 (Thomson Instrument Co., Oceanside, CA), C18, 250 mm × 4.6 mm, particle size 5 μm, eluted with a linear solvent gradient of 5–50 % B over 30 minutes (A = H_2O with 0.1 % TFA, B = MeCN with 0.1 % TFA). HYNIC-**1** was isolated and characterized by ^{1}H NMR and mass spectrometry. Yield: 10.3 ± 2.1%. ^{1}H NMR ($CDCl_3$): δ = 1.92 (4H, m); 3.57 (2H, m); 3.77 (4H, s); 3.86 (8H, s); 4.07 (2H, t); 6.70 (3H, br s); 7.08 (1H, d); 7.35 (8H, m); 7.82 (5H, m); 8.35 (1H, d); 8.75 (4H, d). MS (ESI) m/z (% rel int.): 723.4 (100.0 $[MH]^+$); 745.5 (75.0 $[M+Na]^+$); 362.2 (8.0 $[M+2H]^{2+}$).

4.3. Radiolabeling

4.3.1. $[^{99m}Tc(CO)_3$-1$]^{3+}$—The radiolabeling was accomplished in two steps. First the $[^{99m}Tc(H_2O)_3(CO)_3]^+$ precursor complex was prepared by adding 1 mL of $^{99m}TcO_4^-$ to an Isolink kit and heating for 20 min in boiling water. After cooling, the $[^{99m}Tc(H_2O)_3(CO)_3]^+$ solution (400 μL) was neutralized with 0.1N HCl solution (60μL) and combined with a 1 mM (400 μL) solution of compound **1** in MeCN:phosphate buffered saline, pH 7.4 (PBS) (50:50). The vial was heated to 90 °C for 20 min. Both the labeling precursor $[^{99m}Tc(H_2O)_3(CO)_3]^+$ and$[^{99m}Tc(CO)_3$-**1**$]^{3+}$ were analyzed by RP-HPLC (BioAdvantagePro300 C18 5 μm, 250 mm ×4.6 mm), using a 1 mL/min flow rate and the following gradient: 0-3 min 100 % H_2O with 0.1 % TFA, 3–5 min 100 to 90 % H_2O with 0.1 % TFA, 5–12 min 90 to 0 % H_2O with 0.1 % TFA, 12–25 min 100 % MeCN with 0.1 % TFA. To obtain an injectable solution, the radiolabeling mixture was passed through a C18 Sep-Pak cartridge. The cartridge was washed with water (5 mL), and the radiolabeled compound was eluted with ethanol (1 mL). The ethanol was reduced (< 10 %) by evaporation under a stream of nitrogen and the radiolabeled compound was reconstituted in saline for in vivo use.

4.3.2. ^{99m}Tc-HYNIC-1—The following procedure was used to radiolabel hydrazinonicotinamide conjugated **1** with ^{99m}Tc. To approximately 50 μg of HYNIC-**1** was added 0.5 mL of tricine solution (80 mg/mL in PBS), 100 μL of nicotinic acid solution (20 mg/mL in PBS), 20 μl of $SnCl_2$ H_2O (1 mg/mL in nitrogen purged 0.1N HCl) and 0.3 mL of $^{99m}TcO_4^-$. The mixture was heated for 20 minutes at 90°C. After cooling to room temperature, the reaction mixture was purified by passing it through a C18-Sep-Pak cartridge. The cartridge was washed with water (5 mL) to remove hydrophilic impurities ($^{99m}TcO_4^-$, ^{99m}Tc-co-ligand) and ^{99m}Tc-HYNIC-**1** was eluted with ethanol (1 mL). Ethanol

was evaporated under a stream of N_2 and the radiolabeld compound was redissolved in saline for in vivo evaluation. Radiochemical purity was assessed by analytical RP-HPLC (BioAdvantagePro300 C18 5 μm, 250 mm × 4.6 mm), using a linear solvent gradient of 5–50 % B over 30 minutes (A = H_2O with 0.1 % TFA, B = MeCN with 0.1 % TFA) and a flow rate of 1 mL/min.

4.4. Preparation of Zn-complexes

In all experiments, purified ^{99m}Tc-HYNIC-**1** was complexed with Zn before use. A solution of ^{99m}Tc-HYNIC-**1** in ethanol (1 eq) was mixed with $Zn(NO_3)_2$ (2 eq) and stirred for 15 min at room temperature. For in vivo evaluation, sterile saline was added to reduce the ethanol concentration to < 10%.

4.5. Stability tests

Reverse-phase HPLC analysis (BioAdvantage Pro300, C18, 250 mm × 4.6 mm, particle size 5 μm) was used to determine the stability of the radioligands towards incubation at 37 °C in rat serum and towards incubation at room temperature in saline. Solid-phase extraction (SPE) purified $[^{99m}Tc(CO)_3$-**1**$]^{3+}$ or ^{99m}Tc-HYNIC-**1** was diluted 20-fold in saline or rat serum and incubated at room temperature or 37 °C, respectively. The stability of $[^{99m}Tc(CO)_3$-**1**$]^{3+}$and ^{99m}Tc-HYNIC-**1** was also tested in cysteine solution (100 mM in PBS) at 37 °C. At t = 0 and after 2 h, 4, and 20 h incubation, samples of the solutions were analyzed by RP-HPLC. Gradient elution as described above for $[^{99m}Tc(CO)_3$-**1**$]^{3+}$ and ^{99m}Tc-HYNIC-**1** was used.

4.6. Partition coefficient determination

To determine the partition coefficient ($logD_{n\text{-}octanol/PBS\ pH\ 7.4}$), an aliquot of 20 μL purified $[^{99m}Tc(CO)_3$-**1**$]^{3+}$ or ^{99m}Tc-HYNIC-**1** was added to a test tube containing 0.7 mL *n*-octanol (d = 0.827 g/mL) and 0.7 mL PBS, pH 7.4. The tube was vortexed at room temperature for 2 min and then centrifuged for 10 min at 3000 *g* (Biofuge Pico, Heraeus Instruments, UK). Aliquots of 250 μL of the *n*-octanol and the PBS phase were pipetted into tared test tubes, taking care not to cross-contaminate between the two phases. The samples were weighed and counted for radioactivity in a well counter. Corrections were made for the mass difference and density between the two phases. The partition coefficient D was calculated as: [radioactivity (cpm/mL) in n-octanol/radioactivity (cpm/mL) in PBS]. The logD values are reported as an average of four different measurements.

4.7. Biodistribution study in normal mice

Biodistribution studies of $[^{99m}Tc(CO)_3$-**1**$]^{3+}$and ^{99m}Tc-HYNIC-**1** were performed in normal BALB-c mice (n = 3 per time point) after tail vein injection of 740 kBq of tracer. Mice were sacrificed by ip injection of Beuthanasia-D (Schering-Plough Animal Health Corp., Union, NJ) under isoflurane anesthesia at 15 min, 1 h, 2 h, 4 h or 24 h post tracer injection. Blood was collected and main organs to be examined were removed, rinsed in saline and weighed. Radioactivity of the samples was measured in a well counter (Capintec, Ramsey, NJ). Uptake is expressed as percentage of injected dose (%ID) or percentage of injected dose/g of organ (%ID/g).

4.8. In vivo model of Fas-mediated hepatic apoptosis

To demonstrate in vivo specificity of the tracers for apoptotic cells, an in vivo mouse model of hepatic apoptosis was used. BALB/c mice (n ≥ 4 for each tracer) were injected iv under isoflurane anesthesia with purified hamster anti-Fas mAb (0.22 μg anti-Fas mAb/g body weight, Jo2, BD Pharmingen, San Diego, CA). 90 min later, mice were injected iv with 850 kBq of $[^{99m}Tc(CO)_3$-**1**$]^{3+}$ or ^{99m}Tc-HYNIC-**1.** In parallel, control mice (n ≥ 4 for each

tracer) were injected with the same activity of radioligand. All animals were sacrificed 1 h pi using Beuthanasia-D (100 mg/kg) and dissected. Organs were rinsed in saline to remove blood pool activity and radioactivity was measured in a CRC-15W radioisotope dose calibrator (Capintec, Ramsey, NJ) or in a well counter if activity was < 74 kBq. The uptake of radioactivity is expressed as a percentage of the injected dose per gram of tissue plus or minus the standard deviation (%ID/g tissue ± SD). Livers were quickly frozen and cut into 100 μm thick slices (Cryostat Microm HM 550, Thermo Scientific, Rockford, IL) and thaw-mounted on glass slides for autoradiography.

4.9. In vivo imaging in Fas-mediated hepatic apoptosis

Control and anti-Fas treated mice were imaged on a custom-built planar imaging system (Radiology Department, University of Arizona). The system uses a 25 mm-thick, low-energy parallel-hole collimator with a bore spacing of 1.5-mm attached to a 114 mm-square modular gamma camera. The gamma camera uses a 5 mm-thick NaI(Tl) monolithic scintillation crystal read out by a 3 × 3 array of photomultiplier tubes. Listmode data was collected for 4 minutes and projections were formed using maximum-likelihood position estimation techniques.[46]

4.10. Rat model of myocardial ischemia-reperfusion

A rat model of myocardial ischemia-reperfusion was used to explore uptake of the radioligands in ischemia-reperfusion injury. Myocardial ischemia and reperfusion were produced in male Sprague-Dawley rats (240–280 g) as previously described.[47] The heart was exposed by left thoracotomy. Myocardial ischemia was produced by ligation of the left coronary artery (LCA) for 30 min, followed by 2 h reperfusion. At 2 h of reperfusion, rats were injected iv with 111 MBq of $[^{99m}Tc(CO)_3$-**1**$]^{3+}$ (n = 4) or with ^{99m}Tc-HYNIC-**1** (n = 3). 2 h post tracer injection, rats were injected into the femoral vein with Evans blue (2.5 % in saline, w/v) to delineate the area at risk (unstained) and euthanized using Beuthanasia-D (100 mg/kg). Heart and main organs were rapidly removed, rinsed in saline to remove blood pool activity and blotted dry. Organs were weighed and radioactivity was counted in a dose calibrator or well counter. The heart was quickly frozen and sliced from apex to base, into 2-mm thick transverse sections for autoradiography and histological analysis. The area at risk (AR), which was devoid of Evans Blue, was dissected from the normal myocardium. After weighing the tissues, tracer uptake (%ID/g) in the AR and the normal myocardium (N) was determined by γ-counting in a well counter (Capintec, Ramsey, NJ). From the mean %ID/g values, AR to N uptake ratio (AR/N) was calculated.

4.11. Ex-vivo autoradiography

Autoradiograms were obtained by exposing the tissue sections to a Fujifilm phosphor imaging plate for 15 min (heart slices) or 30 min (liver slices). The images were then scanned at a 50 μm resolution with an 8-bit pixel depth using the FujiFilm BAS5000 Bio-Imaging Analysis System and analyzed using Multi-Gauge 3.0 software.

4.12. Histology

Immediately after harvesting, part of the mouse liver or rat heart slices were fixed in 10 % PBS-buffered formalin for paraffin embedding and histological staining. Routine hematoxylin and eosin (H&E) stains were performed on 3 μm sections of tissue cut from the formalin-fixed, paraffin-embedded (FFPE) blocks. The tissue preparations were examined for morphological evidence of cell death.

4.13. Immunohistochemistry

Detection of apoptotic cells in tissue sections was based on immunohistochemical staining of cleaved caspase-3. For this, rabbit anti-cleaved caspase-3 monoclonal antibody (mAb) (Cell Signaling Technology, Beverly, MA) was used. All steps, including staining of the tissue sections, deparaffinization, and cell conditioning (antigen retrieval with a borate-EDTA buffer) were performed on a Discovery XT Automated Immunostainer (Ventana Medical Systems, Inc, Tucson, AZ), using VMSI-validated reagents. Rabbit anti-cleaved caspase-3 mAb was detected using an anti-rabbit biotinylated secondary mAb followed by biotinylated-streptavidin-horseradish peroxidase and 3,3′-diaminobenzidine system (DAPMap). Primary antibody staining was detected by hematoxylin counterstaining. Following staining, slides were dehydrated through graded alcohols, cleared in xylene and coverslipped with mounting medium. Images were captured using an Olympus BX50 microscope with an Olympus Dp72 camera and CellSense Digital Image software. Images were standardized for light intensity.

4.14. Statistical analysis

Results are expressed as mean ± S.D.. To compare differences between groups, unpaired *t*-test was used. A p-value < 0.05 was considered to indicate statistical significance.

Acknowledgments

The authors would like to thank Dr. Bradley Smith and Dr. Jeffrey Mattis for useful discussions. We are grateful to Stephen Moore and Brian Miller for support in in vivo imaging acquisition, as well as Li Wan for assistance in animal studies. We are thankful to Dr Neil Jacobsen for acquiring the NMR data. We also acknowledge Covidien for kindly providing us with Isolink kits. We thank Edward Abril from Tissue Acquisition and Cellular/Molecular Analysis Shared Service (TACMASS), which is supported by the Arizona Cancer Center Support Grant (NIH CA023074), for generating the immunohistochemical and histological data. This study was supported by NIH grants NHLBI R01-HL090716 and NIBIB P41-EB002035.

References

1. Roshal M, Zhu Y, Planelles V. Apoptosis. 2001; 6:103. [PubMed: 11321033]
2. Miller LW, Granville DJ, Narula J, McManus BM. Cardiol Clin. 2001; 19:141. [PubMed: 11787808]
3. Yuan J, Yankner BA. Nature. 2000; 407:802. [PubMed: 11048732]
4. Krijnen P, Nijmeijer R, Meijer C, Visser C, Hack C, Niessen H. J Clin Pathol. 2002; 55:801. [PubMed: 12401816]
5. Cotter TG. Nature Rev Cancer. 2009; 9:501. [PubMed: 19550425]
6. Rishi AK, Zhang X, Wali A. Pharm Persp Cancer Therap. 2009; 149
7. De Saint-Hubert M, Prinsen K, Mortelmans L, Verbruggen A, Mottaghy FM. Methods. 2009; 48:178. [PubMed: 19362149]
8. Fadok VA, Voelker DR, Campbell PA, Cohen JJ, Bratton DL, Henson PM. J Immunol. 1992; 148:2207. [PubMed: 1545126]
9. Blankenberg FG. J Nucl Med. 2008; 49:81S. [PubMed: 18523067]
10. Martin SJ, Reutelingsperger C, McGahon AJ, Rader JA, Van Schie R, LaFace D, Green D. J Exp Med. 1995; 182:1545. [PubMed: 7595224]
11. Savill J, Fadok V, Henson P, Haslett C. Immunol Today. 1993; 14:131. [PubMed: 8385467]
12. Hanshaw RG, Smith BD. Bioorg Med Chem. 2005; 13:5035. [PubMed: 15914007]
13. Vermes I, Haanen C, Steffens-Nakken H, Reutelingsperger C. J Immunol methods. 1995; 184:39. [PubMed: 7622868]
14. Gerke V, Moss S. Physiol Rev. 2002; 82:331. [PubMed: 11917092]
15. Murakami Y, Takamatsu H, Taki J, Tatsumi M, Noda A, Ichise R, Tait JF, Nishimura S. Eur J Nucl Med Mol Imaging. 2004; 31:469. [PubMed: 14666384]

16. Bauwens M, Saint-Hubert M, Devos E, Deckers N, Reutelingsperger C, Mortelmans L, Himmelreich U, Mottaghy FM, Verbruggen A. Nucl Med Biol in press.
17. Keen HG, Dekker BA, Disley L, Hastings D, Lyons S, Reader AJ, Ottewell P, Watson A, Zweit J. Nucl Med Biol. 2005; 32:395. [PubMed: 15878509]
18. Lahorte C, Dumont F, Slegers G, Van De Wiele C, Dierckx R, Philippe J. J Lab Comp Radioph. 2000; 43:739.
19. De Saint-Hubert M, Mottaghy FM, Vunckx K, Nuyts J, Fonge H, Prinsen K, Stroobants S, Mortelmans L, Deckers N, Hofstra L, Reutelingsperger CPM, Verbruggen A, Rattat D. Biorg Med Chem. 2010; 18:1356.
20. Koulov A, Stucker K, Lakshmi C, Robinson J, Smith B. Cell Death Differ. 2003; 10:1357. [PubMed: 12970674]
21. Hanshaw RG, Smith BD. Bioorg Med Chem. 2005; 13:5035. [PubMed: 15914007]
22. Smith BA, Akers WJ, Leevy WM, Lampkins AJ, Xiao S, Wolter W, Suckow MA, Achilefu S, Smith BD. J Am Chem Soc. 2009; 132:67. [PubMed: 20014845]
23. Leevy WM, Gammon ST, Jiang H, Johnson JR, Maxwell DJ, Jackson EN, Marquez M, Piwnica-Worms D, Smith BD. J Am Chem Soc. 2006; 128:16476. [PubMed: 17177377]
24. Leevy WM, Gammon ST, Johnson JR, Lampkins AJ, Jiang H, Marquez M, Piwnica-Worms D, Suckow MA, Smith BD. Bioconj Chem. 2008; 19:686.
25. He X, Gao J, Gambhir SS, Cheng Z. Trends Mol Med. 2010; 16:574. [PubMed: 20870460]
26. Ferreira CL, Marques FLN, Okamoto MRY, Otake AH, Sugai Y, Mikata Y, Storr T, Bowen M, Yano S. App l Radiat Isot. 2010; 68:1087.
27. Maresca KP, Hillier SM, Femia FJ, Zimmerman CN, Levadala MK, Banerjee SR, Hicks J, Sundararajan C, Valliant J, Zubieta J. Bioconjug Chem. 2009; 20:1625. [PubMed: 19572702]
28. Meszaros LK, Dose A, Biagini SCG, Blower PJ. Inorg Chim Acta. 2010; 363:1059.
29. Faintuch B, Santos R, Souza A, Hoffman T, Greeley M, Smith C. Synth React Inorg Met-Org Nano-Met Chem. 2005; 35:43.
30. Liu G, Wescott C, Sato A, Wang Y, Liu N, Zhang YM, Rusckowski M, Hnatowich DJ. Nucl Med Biol. 2002; 29:107. [PubMed: 11786281]
31. Ballinger JR, Cooper MS, Mather SJ. Eur J Nucl Med Mol Imaging. 2004; 31:304. [PubMed: 15129716]
32. Maresca KP, Marquis JC, Hillier SM, Lu G, Femia FJ, Zimmerman CN, Eckelman WC, Joyal JL, Babich JW. Bioconjug Chem. 2010; 21:1032. [PubMed: 20402463]
33. Aloya R, Shirvan A, Grimberg H, Reshef A, Levin G, Kidron D, Cohen A, Ziv I. Apoptosis. 2006; 11:2089. [PubMed: 17051335]
34. Ogasawara J, Watanabe-Fukunaga R, Adachi M, Matsuzawa A, Kusagai T, Kitamura Y, Itoh N, Suda T, Nagata S. Nature. 1993; 364:806. [PubMed: 7689176]
35. Blankenberg FG, Katsikis PD, Tait JF, Davis RE, Naumovski L, Ohtsuki K, Kopiwoda S, Abrams MJ, Darkes M, Robbins RC, Maecker HT, Strauss HW. Proc Natl Acad Sci USA. 1998; 95:6349. [PubMed: 9600968]
36. Ashkenazi A, Dixit VM. Curr Opin Cell Biol. 1999; 11:255. [PubMed: 10209153]
37. Luo Q, Zhang Z, Wang F, Lu H, Guo Y, Zhu R. Biochem Biophys Res Commun. 2005; 335:1102. [PubMed: 16105648]
38. DiVittorio KM, Johnson JR, Johansson E, Reynolds AJ, Jolliffe KA, Smith BD. Org Biomol Chem. 2006; 4:1966. [PubMed: 16688342]
39. Piot C, Martini JF, Bui SK, Wolfe CL. Cardiovasc Res. 1999; 44:536. [PubMed: 10690285]
40. Sarda-Mantel L, Hervatin F, Michel J, Louedec L, Martet G, Rouzet F, Lebtahi R, Merlet P, Khaw B, Le Guludec D. Eur J Nucl Med Mol Imaging. 2008; 35:158. [PubMed: 17805532]
41. Kenis H, Zandbergen HR, Hofstra L, Petrov AD, Dumont EA, Blankenberg FD, Haider N, Bitsch N, Gijbels M, Verjans JWH, Narula N, Narula J, Reutelingsperger CPM. J Nucl Med. 2010; 51:259. [PubMed: 20124049]
42. Taki J, Higuchi T, Kawashima A, Tait JF, Kinuya S, Muramori A, Matsunari I, Nakajima K, Tonami N, Strauss HW. J Nucl Med. 2004; 45:1536. [PubMed: 15347721]

43. Saeed M, Dijke CF, van Mann JS, Wendland MF, Rosenau W, Higgins CB, Brasch RC. J Magn Res Imaging. 1998; 8:561.

44. Zhao M, Zhu X, Ji S, Zhou J, Ozker KS, Fang W, Molthen RC, Hellman RS. J Nucl Med. 2006; 47:1367. [PubMed: 16883018]

45. Lakshmi C, Hanshaw RG, Smith BD. Tetrahedron. 2004; 60:11307.

46. Hesterman JY, Caucci L, Kupinski MA, Barrett HH, Furenlid LR. Nucl Sci, IEEE Trans. 2010; 57:1077.

47. Liu Z, Chen L, Liu S, Barber C, Stevenson GD, Furenlid LR, Barrett HH, Woolfenden JM. J Nucl Cardiol. 2010; 17:858. [PubMed: 20669059]

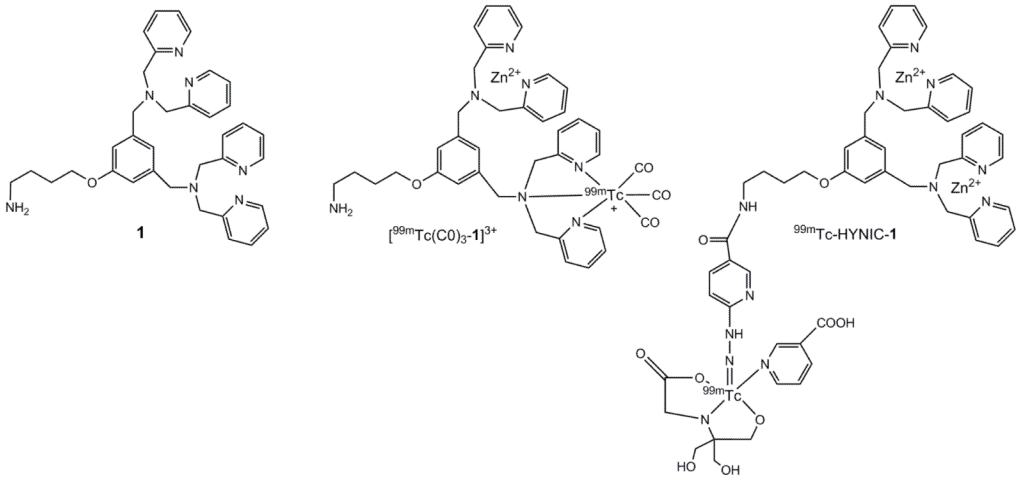

Figure 1.
Structure of compound **1** and putative structures of $[^{99m}Tc(CO)_3$-**1**$]^{3+}$ and ^{99m}Tc-HYNIC-**1**, complexed with Zn^{2+}.

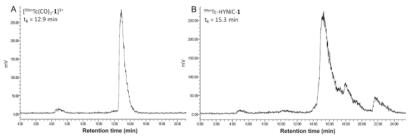

Figure 2.
Representative radiochromatograms of $[^{99m}Tc(CO)_3$-**1**$]^{3+}$ (A) and ^{99m}Tc-HYNIC-**1** (B) before C18 Sep-Pak purification.

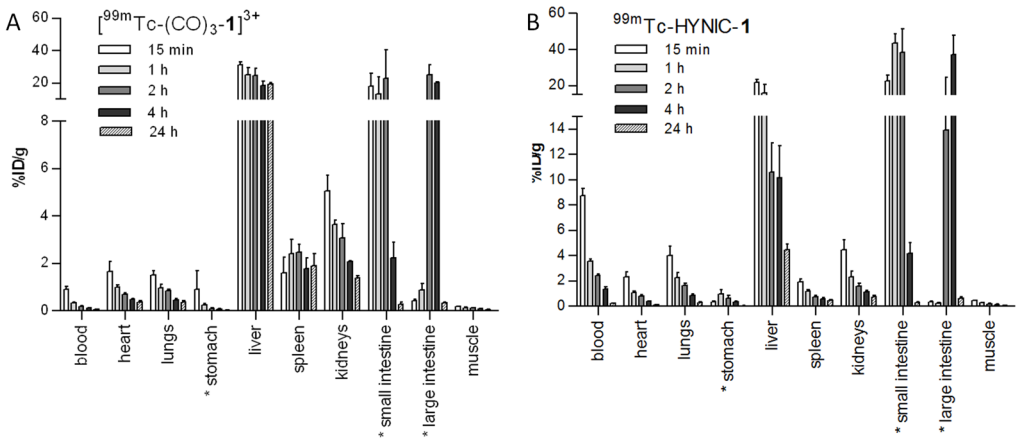

Figure 3.

Tissue distribution (%ID/g) at different time points post injection of $[^{99m}Tc(CO)_3$-**1**$]^{3+}$ (A) or ^{99m}Tc-HYNIC-**1** (B) in normal BALB-c mice (n = 3 per time point).

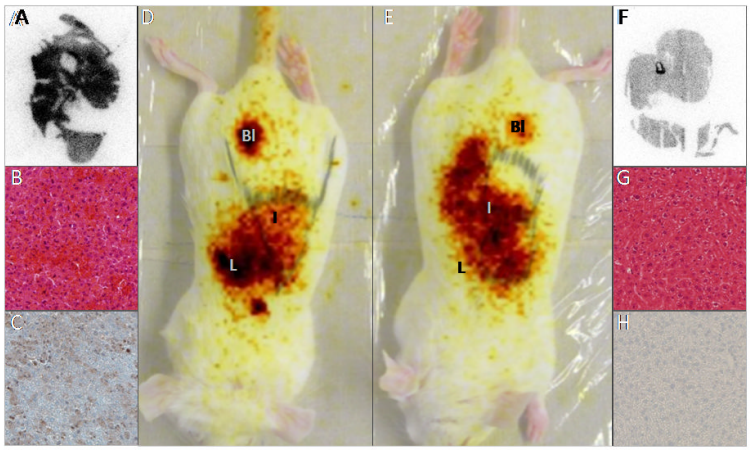

Figure 4.

Planar images 50 min after ^{99m}Tc-HYNIC-**1** injection in anti-Fas treated (D) or normal mice (E). Liver, intestines and bladder are indicated by L, I and Bl. 60 min pi livers were excised, and analyzed by autoradiography (A: anti-Fas treated, F: normal), H&E (B:anti-Fas treated, G: normal) and immunostaining (C: anti-Fas treated, H: normal) using an anti-cleaved caspase-3 mAb (brown color in C).

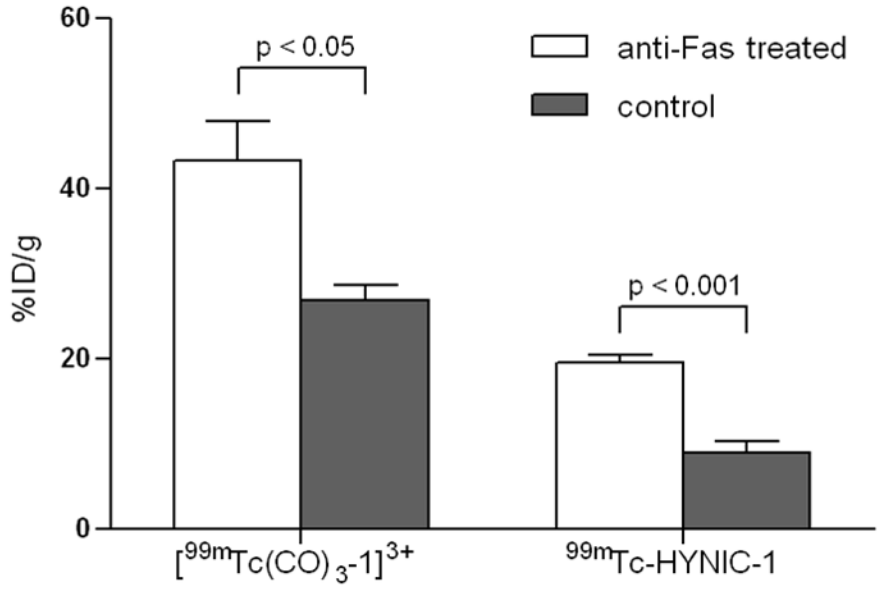

Figure 5.

Uptake of radioactivity (%ID/g) in livers of control mice or mice treated with anti-Fas mAb, 60 min post iv injection of $[^{99m}Tc(CO)_3$-**1**$]^{3+}$ and ^{99m}Tc-HYNIC-**1**.

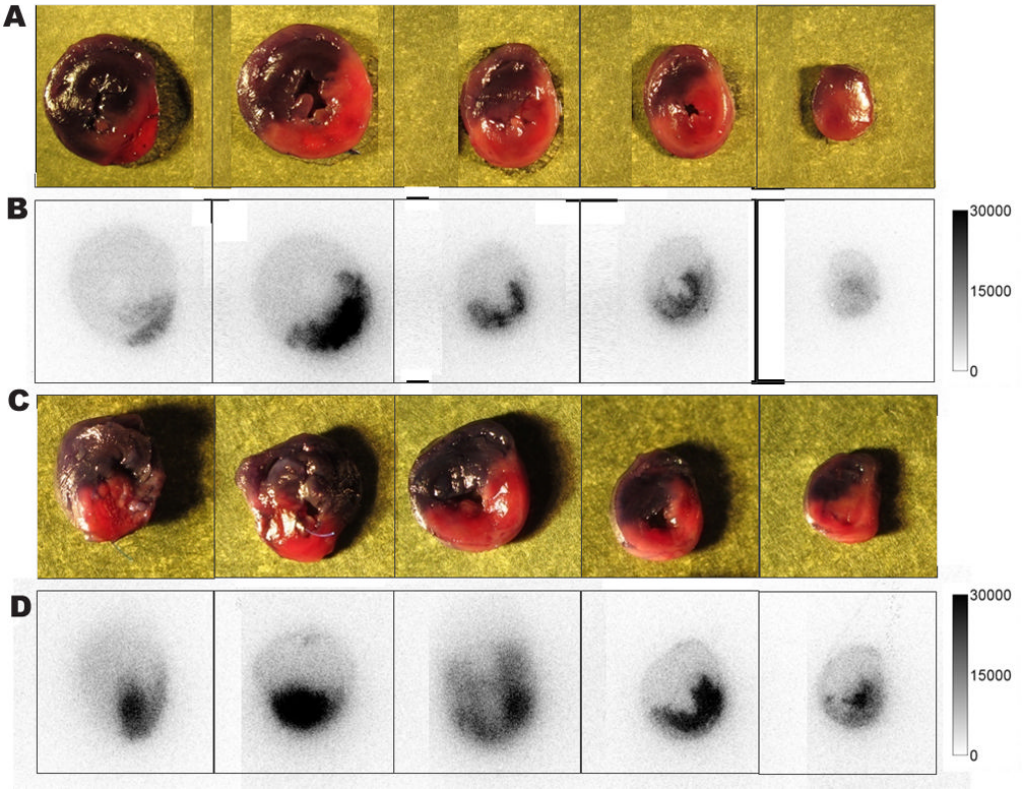

Figure 6.

Digital photographs of 2mm myocardial slices from rats injected iv with 111 MBq of $[^{99m}Tc(CO)_3$-**1**$]^{3+}$ (A) or with ^{99m}Tc-HYNIC-**1** (C). Normal myocardium is colored with Evans blue (blue-grey zones); the area at risk is pink-red. Corresponding autoradiograms with $[^{99m}Tc(CO)_3$-**1**$]^{3+}$ (B) or ^{99m}Tc-HYNIC-**1** (D) uptake matching the area at risk.

Table 1

Stability of [^{99m}Tc(CO)$_3$-**1**]$^{3+}$ and ^{99m}Tc-HYNIC-**1** in aqueous solutions

	Duration of incubation			
	0 h	**2 h**	**4 h**	**20 h**
[^{99m}Tc(CO)$_3$-**1**]$^{3+}$ (%)				
Saline	99.9	99.9	99.9	99.9
Serum	99.9	99.9	99.9	98.2
Cysteine	99.9	99.9	99.9	99.9
^{99m}Tc-HYNIC-**1** (%)				
Saline	77.7	75.9	74.8	72.1
Serum	82.3	81.5	80.7	66.7
Cysteine	80.7	80.5	80.4	56.3

nd not determined